A High Performance Pneumatic Force Actuator System: Part II—Nonlinear Controller Design

Article *in* Journal of Dynamic Systems Measurement and Control · September 2000

DOI: 10.1115/1.1286366

2 authors:

Edmond Richer
Southern Methodist University
70 PUBLICATIONS **1,735** CITATIONS

SEE PROFILE

Yildirim Hurmuzlu
Southern Methodist University
80 PUBLICATIONS **3,045** CITATIONS

SEE PROFILE

A High Performance Pneumatic Force Actuator System: Part II—Nonlinear Controller Design

Edmond Richer[1]

Yildirim Hurmuzlu

Southern Methodist University,
School of Engineering and Applied Science,
Mechanical Engineering Department,
Dallas, TX 75275

In this article we present two nonlinear force controllers based on the sliding mode control theory. For this purpose we use the detailed mathematical model of the pneumatic system developed in the first part of the paper. The first controller is based on the complete model, and exhibits superior performance both in the numerical simulation and experiments, but requires complex online computations for the control law. The second controller neglects the valve dynamics and the time delay due to connecting tubes. The performance of this controller exhibits slight degradation for configurations with relatively short tubes, and at frequencies up to 20 Hz. At higher frequencies or when long connecting tubes are used, however, the performance exhibits significant degradation compared to the one provided by the full order controller. [S0022-0434(00)00703-6]

1 Introduction

Pneumatic actuators are often used in applications that require high power-to-weight ratio, combined with low price and clean operation. Unfortunately, due to the compressibility of air, highly nonlinear behavior, and time delay due to slow propagation of pressure waves position and force control of these actuators are difficult. During the past decade, researchers have tried controlling the pneumatic actuators using different approaches. Mannetje [1] obtained a 10 Hz bandwidth using a PD *pressure* controller and a specially designed valve directly attached to the cylinder. Bobrow and Jabbari [2] used an adaptive controller based on linearized dynamics about the operating point. They reported good results for a 2 Hz, low amplitude sinusoidal wave when the operating point was close to the midstroke position. Their reported performance was significantly affected at the end of the piston's strokes. Ferraresi et al. [3] and McDonnel and Bobrow [4] also used adaptive control for force actuation and trajectory tracking. Yet their results were restricted to frequency range with an approximately 1 Hz upper limit. Ben-Dov and Salcudean [5] developed a liner force controller for a pneumatic actuator that included two low-friction glass cylinders, each connected by a *short* tube to a custom built flapper valve. Their model included the valve dynamics and a linearized valve flow equation. The experimental results exhibited a bandwidth of 16 Hz for forces in the range of ± 2 N and 8 Hz in the range of ± 8.15 N. Richard and Scavarda [6] obtained only a limited improvement in performance using a nonlinear controller. The rise time with step input experiments was larger than 0.300 s. Sliding mode controllers were also developed by Arun et al. [7], Thang and Walker [8], Pandian et al. [9]. These controllers however are strictly position controllers that achieve improved performances at low frequencies.

The objective of this article is to design a high performance force controller, suitable for very demanding applications such as haptic interfaces. The main goal is to achieve significantly wider frequency bandwidths at higher force levels under more realistic design configurations. This includes longer tube lengths, commercially available components, etc. Such requirements often arise in practical applications in robotics and automation. The linear control techniques based on relatively simple mathematical models, and even the more sophisticated approaches such as adaptive control fail to provide this level of performance. We choose the Sliding Mode Control (SMC) theory for nonlinear force control implementation, considering its robustness and high performance characteristics even for highly nonlinear systems.

We developed two force controllers in this study. The first force controller was designed using the detailed mathematical model developed in the first part of the article. It provides excellent performance both in the numerical simulation and experiments, but requires complex online computations. The second controller uses a reduced order model obtained by neglecting the valve dynamics and the time delay induced by the connecting tubes. The control law is greatly simplified, and the performance is only slightly altered up to frequencies of 20 Hz. For higher frequencies and especially in configurations with long connecting tubes, however, the full order controller performed significantly better. We should note that even the full order controller can be practically implemented with the readily available hardware components. Yet, one may use the second controller in less demanding applications to have a simpler control scheme. Both controllers exhibit greatly improved performances in comparison to the previously published results.

2 Pneumatic System Model

A pneumatic cylinder controlled by a proportional valve can be modeled using four differential equations: an equation for the piston-load dynamics, two equations for the rate of change of pressure in individual chambers, and one equation for the valve dynamics (see Richer and Hurmuzlu [10]). The differential equation describing the piston-load dynamics is given by

$$(M_L + M_p)\ddot{x} = P_1 A_1 - P_2 A_2 - P_a A_r - \beta \dot{x} - F_f - F_L \qquad (1)$$

where M_L is the external load mass, M_p is the piston and rod assembly mass, x is the piston position relative to the middle of the stroke, P_1 and P_2 are the absolute pressures in actuator's chambers, P_a is the absolute ambient pressure, A_1 and A_2 are the piston effective areas, A_r is the rod area, β is the viscous friction coefficient, F_f is the Coulomb friction force, and F_L is the external load force.

As we have shown in Richer and Hurmuzlu [10] the rates of change of the pressures in the chambers can be expressed as

[1]Presently with Advanced Radiological Sciences in the University of Texas Southwestern Medical Center at Dallas.

Contributed by the Dynamic Systems and Control Division for publication in the JOURNAL OF DYNAMIC SYSTEMS, MEASUREMENT, AND CONTROL. Manuscript received by the Dynamic Systems and Control Division June 23, 1999. Associate Technical Editor: S. Nair.

$$\dot{P}_1=\frac{C_f R\sqrt{T}}{V_{01}+A_1\left(\frac{1}{2}L+x\right)}[\alpha_{\text{in}}\phi_{\text{in}_1}\overline{A}_{v1_{\text{in}}}P_s\dot{m}_r(P_s,\overline{P}_1)$$

$$-\alpha_{\text{ex}}\phi_{\text{ex}}\overline{A}_{v1_{\text{ex}}}\overline{P}_1\dot{m}_r(\overline{P}_1,P_a)]-\alpha\frac{P_1A_1}{V_{01}+A_1\left(\frac{1}{2}L+x\right)}\dot{x} \tag{2}$$

$$\dot{P}_2=\frac{C_f R\sqrt{T}}{V_{02}+A_2\left(\frac{1}{2}L-x\right)}[\alpha_{\text{in}}\phi_{\text{in}_2}\overline{A}_{v2_{\text{in}}}P_s\dot{m}_r(P_s,\overline{P}_2)$$

$$-\alpha_{\text{ex}}\phi_{\text{ex}_2}\overline{A}_{v2_{\text{ex}}}\overline{P}_2\dot{m}_r(\overline{P}_2,P_a)]+\alpha\frac{P_2A_2}{V_{02}+A_2\left(\frac{1}{2}L-x\right)}\dot{x} \tag{3}$$

where C_f is a nondimensional discharge coefficient, R is the ideal gas constant, T is the air temperature, P_s is the pressure in the air supply reservoir, V_{0i} is the inactive volume at the end of stroke and admission ports, L is the piston stroke, α_{in} and α_{ex} are the heat transfer coefficients for compression (input path) and expansion (exhaust path), ϕ_{in} and ϕ_{ex} are the connecting tubes attenuation coefficients, $\overline{A}_{vi_{\text{in}}}$ and $\overline{A}_{vi_{\text{ex}}}$ are the delayed valve areas for the input and exhaust paths, and $\dot{m}_r(P_u,P_d)$ is the reduced flow function, here P_u and P_d are being the valve upstream and downstream pressures. The expressions for attenuation coefficients and induced time delay in the connecting tubes, valve areas versus spool displacement, and the reduced flow function are presented in Richer and Hurmuzlu [10].

The dynamical model for the spool proportional valve with the friction neglected (assuming dithered spool) is,

$$M_s\ddot{x}_s=-c_s\dot{x}_s-2k_sx_s+K_{fc}i_c \tag{4}$$

where M_s is the valve spool mass, x_s is the spool displacement from central (closed) position, c_s is the spool viscous damping coefficient, k_s is the springs constant, K_{fc} is the coil force coefficient, and i_c is the coil current.

Figure 1 depicts a schematic representation of the pneumatic actuator system, including pneumatic cylinder, control valve, connecting tubes, position transducer, and pressure sensors.

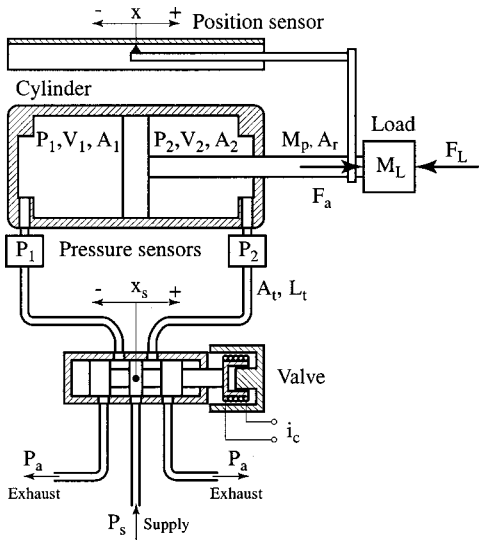

Fig. 1 Schematic representation of the pneumatic cylinder-valve system

3 Controller Design

The output of interest of the pneumatic system is the force produced by the actuator, F_a (see Fig. 1). We can obtain the expression for F_a from Eq. (1), eliminating the terms related to the external load,

$$F_a=P_1A_1-P_2A_2-P_aA_r-\beta\dot{x}-F_f \tag{5}$$

where we neglect the inertia of the piston, assuming $M_L\gg M_p$ for most applications. The control problem is to get the actuator output force F_a to track a specific time varying force F_d. Accordingly, the tracking error will be,

$$\tilde{F}=F_a-F_d. \tag{6}$$

3.1 Sliding Mode Controller. Using the tracking error from Eq. (6) we define a time-varying surface $S(t)$, such that

$$S(t)=\left(\frac{d}{dt}+\lambda\right)^{n-1}\tilde{F} \tag{7}$$

where λ is a strictly positive constant, and n is the number of differentiations required for the controller input to appear in the sliding mode dynamics. Thus, the problem of tracking the desired force F_d is equivalent to a first order stabilization problem in s. The right-hand side of Eq. (7) includes the second derivatives of the desired and actuator forces. In addition, the sliding mode scheme necessitates the computation of $\dot{s}$ and thus the third derivatives of the two forces. In order to eliminate the third-order derivatives from the control law, the valve dynamics can be approximated using a first-order differential equation. This can be achieved by neglecting the inertial term $M_s\ddot{x}_s$ in Eq. (4). We justify this assumption by considering that the spool inertial force is much smaller than the force applied by the internal springs of the valve. Accordingly, we may write

$$\dot{x}_s=-\frac{1}{\tau_v}x_s+\frac{1}{\tau_v}u \tag{8}$$

where $\tau_v=c_s/(2k_s)$ and the control input is given by

$$u=\frac{K_{fc}}{2k_s}i_c. \tag{9}$$

Thus, the sliding function s can be written as

$$s=\dot{\tilde{F}}+\lambda\tilde{F}. \tag{10}$$

Substituting $\tilde{F}$ from Eq. (6) and using F_a from Eq. (5) we obtain

$$s=\lambda(A_1P_1-A_2P_2-A_rP_a-F_f-F_d)$$
$$+A_1\dot{P}_1-A_2\dot{P}_2-\dot{F}_d-\lambda\beta\dot{x}-\beta\ddot{x}. \tag{11}$$

Differentiating Eq. (11) with respect with time yields

$$\dot{s}=\lambda(A_1\dot{P}_1-A_2\dot{P}_2-\dot{F}_d)+A_1\ddot{P}_1-A_2\ddot{P}_2-\ddot{F}_d-\lambda\beta\ddot{x}-\beta x^{(3)}. \tag{12}$$

Now we obtain the equivalent control, u_{eq} by setting Eq. (12) equal to zero and solving for u. The detailed derivations to obtain u_{eq} is presented in the Appendix.

The control law now can be written as follows

$$u=u_{eq}-\kappa\,\text{sat}(s/\Psi) \tag{13}$$

where κ is the controller gain defined as a function of the state variables, Ψ is the thickness of a thin boundary layer introduced to avoid chattering, and sat is the saturation function,

$$\text{sat}(y)=\begin{cases}-1 & \text{if } y<-1\\ y & \text{if } |y|\leqslant 1\\ +1 & \text{if } y>+1\end{cases}. \tag{14}$$

The constant λ that appears in the sliding function (Eq. (10)), represents the controller bandwidth. It should be set equal to a large value for high tracking performance. As it is shown in Slotine and Li [11] its value is typically limited by the lowest unmodeled structural mode, unmodeled time delays, and controller sampling rate. We found that the latter condition is the most restrictive. Considering the full cycle frequency of the controller ω_s

$$\lambda \leqslant \lambda_s \approx \frac{1}{5}\omega_s. \tag{15}$$

The controller gain, κ, from Eq. (13) was chosen such that it is approximately (without the dissipation terms) proportional to the actuator output force,

$$\kappa = \kappa_0 + \kappa_1(A_1P_1 - A_2P_2 - A_rP_a). \tag{16}$$

The optimum values for the constants κ_0 and κ_1 can be determined experimentally. Also, for simplicity, we choose a constant boundary layer thickness in the following form

$$\Psi = \lambda \tilde{F}_{ad} \tag{17}$$

where $\tilde{F}_{ad}$ is a constant *admissible force error*.

3.2 Reduced Order Controller. The control law derived in the previous section is complex and can be justified in some applications with very stringent requirements. For less demanding tasks, however, a simpler controller may provide satisfactory results. Thus, in this section we simplify the control law to achieve this objective.

Neglecting the valve dynamics and the time delay induced by the valve-cylinder connecting tubes, the mathematical model of the pneumatic cylinder will become a first-order system ($n=1$). The sliding function s can now be written as

$$s = \tilde{F} = P_1A_1 - P_2A_2 - P_aA_r - \beta\dot{x} - F_d \tag{18}$$

and the sliding mode equation becomes

$$\dot{s} = \dot{P}_1A_1 - \dot{P}_2A_2 - \beta\ddot{x} - \dot{F}_d. \tag{19}$$

Substituting the derivatives of the pressures from Eqs. (2) and (3) into (19), neglecting the time delay, and using the symmetry of the valve areas for the two cylinder chambers from Eqs. (37) and (38) yields

$$\begin{aligned}\dot{s} = {} & A_{v_{\text{in}}}K_f\left(\frac{A_1P_s\alpha_{\text{in}}\phi_{\text{in}}\dot{m}_r(P_s,P_1)}{V_1} + \frac{A_2P_2\alpha_{\text{ex}}\phi_{\text{ex}}\dot{m}_r(P_2,P_a)}{V_2}\right) \\ & - A_{v_{\text{ex}}}K_f\left(\frac{A_1P_1\alpha_{\text{ex}}\phi_{\text{ex}}\dot{m}_r(P_1,P_a)}{V_1} + \frac{A_2P_s\alpha_{\text{in}}\phi_{\text{in}}\dot{m}_r(P_s,P_2)}{V_2}\right) \\ & - \alpha\left(\frac{A_1^2P_1}{V_1} + \frac{A_2^2P_2}{V_2}\right)\dot{x} - \beta\ddot{x} - \dot{F}_d.\end{aligned} \tag{20}$$

We compute the equivalent control u_{eq} by setting Eq. (20) equal to zero. The resulting equation can be solved for the equivalent values of the input and exhaust valve areas: $A_{v_{\text{in}}}^{eq}$ and $A_{v_{\text{ex}}}^{eq}$. Using Fig. 6 in Richer and Hurmuzlu [10] we may write the following equation,

$$A_{v_{\text{in}}}^{eq}A_{v_{\text{ex}}}^{eq} = 0. \tag{21}$$

In addition, we may formulate the following conditions on the two valve areas:

1 if $s<0$ the force provided by the actuator needs to be increased, and the air should flow in the first cylinder chamber
2 if $s>0$ force provided by the actuator needs to be decreased, and the air should flow in the second cylinder chamber

Now, combining Eqs. (20), (21) and the the two conditions, we may write,

$$A_{v_{\text{in}}}^{eq} = \begin{cases} \dfrac{V_1V_2(\beta\ddot{x} + \dot{F}_d) + \alpha(V_2A_1^2P_1 + V_1A_2^2P_2)\dot{x}}{K_f[V_2A_1P_s\alpha_{\text{in}}\phi_{\text{in}}\dot{m}_r(P_s,P_1) + V_1A_2P_2\alpha_{\text{ex}}\phi_{\text{ex}}\dot{m}_r(P_2,P_a)]} & \text{if } s<0 \\ 0 & \text{if } s\geqslant 0 \end{cases} \tag{22}$$

$$A_{v_{\text{ex}}}^{eq} = \begin{cases} -\dfrac{V_1V_2(\beta\ddot{x} + \dot{F}_d) + \alpha(V_2A_1^2P_1 + V_1A_2^2P_2)\dot{x}}{K_f[V_2A_1P_1\alpha_{\text{ex}}\phi_{\text{ex}}\dot{m}_r(P_1,P_a) + V_1A_2P_s\alpha_{\text{in}}\phi_{\text{in}}\dot{m}_r(P_s,P_2)]} & \text{if } s>0 \\ 0 & \text{if } s\leqslant 0 \end{cases}. \tag{23}$$

The equivalent valve areas can be used to compute the corresponding spool displacement, which is used to compute the required coil current. The valve area expressions (see Richer and Hurmuzlu [10]) involve complex trigonometric and algebraic functions, thus the computation of a closed form inverse function for the spool displacement is not possible. In order to overcome this difficulty, the expressions for the areas of the valve were approximated using fractional power series, which can be represented as follows (obtained by using Mathematica)

$$\begin{aligned}{}^sA_v(x_e) = {} & n_h\sqrt{2}\left(\frac{4}{3}R_h^{1/2}x_e^{3/2} - \frac{1}{5}R_h^{-1/2}x_e^{5/2}\right. \\ & \left. - \frac{1}{56}R_h^{-3/2}x_e^{7/2} - \frac{1}{288}R_h^{-5/2}x_e^{9/2}\right) + O(x_e)^5\end{aligned} \tag{24}$$

where ${}^sA_v(x_e)$ is the approximated valve area as a function of spool effective displacement x_e (see Richer and Hurmuzlu [10] Eq. (43)), R_h is the radius of the holes, n_h is the number of holes in one valve air path. Valve areas for $R_h<x_e<2R_h$ are computed from Eq. (24) by using the central symmetry as shown in Fig. 2. Figure 2 depicts the valve area and its series approximations using two, three, and four terms. The corresponding approximation errors are also plotted. The error for the three terms approximation is less than 0.1 mm^2, which is sufficiently small for all practical purposes.

The effective spool displacement is obtained by inverse series expansion in the following form

$$\begin{aligned}{}^sx_e(A_v) = {} & \frac{\left(\frac{3}{2}\right)^{2/3}A_v^{2/3}}{2n_h^{2/3}R_h^{1/3}} + \frac{3\left(\frac{3}{2}\right)^{1/3}A_v^{4/3}}{80n_h^{4/3}R_h^{5/3}} + \frac{99A_v^2}{11200n_h^2R_h^3} \\ & + \frac{823\left(\frac{3}{2}\right)^{2/3}A_v^{8/3}}{448000n_h^{8/3}R_h^{13/3}} + O(A_v)^{10/3}.\end{aligned} \tag{25}$$

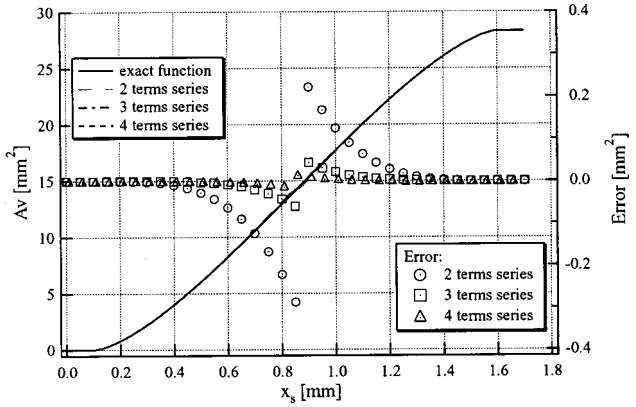

Fig. 2 Series approximation of the valve area, and the approximation error for 2, 3, and 4 terms in the series

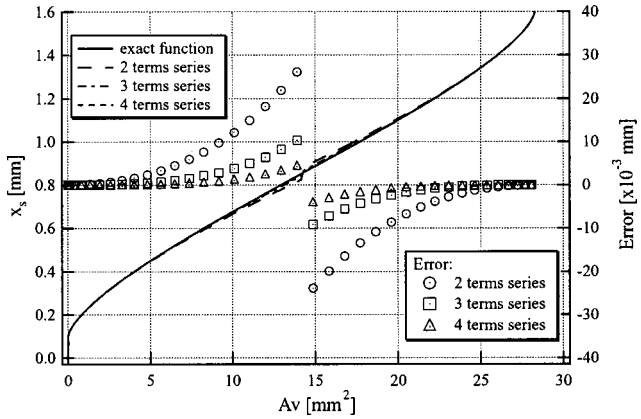

Fig. 3 Series approximation of the spool displacement, and the approximation error for 2, 3, and 4 terms in the series

Here, we use the central symmetry to obtain the absolute spool displacement as follows,

$$x_s(A_v)=\begin{cases}0 & \text{if } A_v=0\\ p_w-R_h+{}^s x_e(A_v) & \text{if } A_v\leqslant A_{v_{\max}}/2\\ p_w+R_h-{}^s x_e(A_{v_{\max}}-A_v) & \text{if } A_v\leqslant A_{v_{\max}}\end{cases} \quad (26)$$

where $2p_w$ is the spool width, and $A_{v_{\max}}=n_h\pi R_h^2$ is the maximum valve area. The approximations depicted in Fig. 3 show that using three terms in the series produces an error less than 10 μm. Thus, we use three terms series to approximate the spool displacement.

Finally, the equivalent control can be written as follows,

$$u_{eq}=\begin{cases}x_s(A_{v_{\text{in}}}^{eq}) & \text{if } s<0\\ 0 & \text{if } s=0\\ -x_s(A_{v_{\text{ex}}}^{eq}) & \text{if } s>0.\end{cases} \quad (27)$$

The complete control law given by Eq. (13), includes the additional term $\kappa\ \text{sat}(s/\Psi)$, which compensates for model imprecisions. In the case of the simplified controller, the gain κ and the boundary layer thickness Ψ can simply be chosen as constants.

4 Numerical Simulation and Experimental Validation

The mathematical model of the pneumatic system presented in Section 2 was verified numerically and experimentally in the first part of this paper. Also, the variables that are dependent on the geometric and structural characteristics of the pneumatic cylinder, valve, and the connecting tubes were identified using relatively simple experiments designed for this purpose. This section is concerned with numerical and experimental validation of the two nonlinear controllers that were presented earlier in the article. The performance of the reduced order controller is compared to that of the full order sliding mode controller for different control tasks and plant parameters. We are particularly interested in the frequency response and the loss in performance when long connection tubes between valve and cylinder are used.

4.1 Numerical Verification. The differential equations describing the pneumatic system, Eqs. (1)–(4), and the equations that constitute the two control laws were implemented by using *Mathematica 3.01* symbolic modules. Two sets of simulation runs were conducted. In each case the piston was fixed at the middle of the stroke. The first set of simulations was conducted with two different tube lengths and using the full order controller. The second set was also carried out using two different tube lengths, but using the reduced order controller. In all simulation runs we chose a sinusoidal desired force with an amplitude and frequency of 75 N and 20 Hz, respectively. Figures 4 and 5 depict the outcomes of the simulation runs obtained by using the full order sliding mode controller, and connecting tubes of 0.5 m and 2 m, respectively. Figures 4(a) and 5(a) depict the desired and actual actuator forces. Figures 4(b) and 5(b) depict the applied control inputs and the valve displacements. In both cases the full order SMC attained the desired response within 30 ms and achieved almost perfect tracking. The sharp peaks in the control law that can be observed from the figure correspond to regions of flow reversal in the cylinder chambers. The effect of these peaks is not significant because their influence was eventually filtered out from the system response (see the spool displacement in Figs. 4(b) and 5(b)).

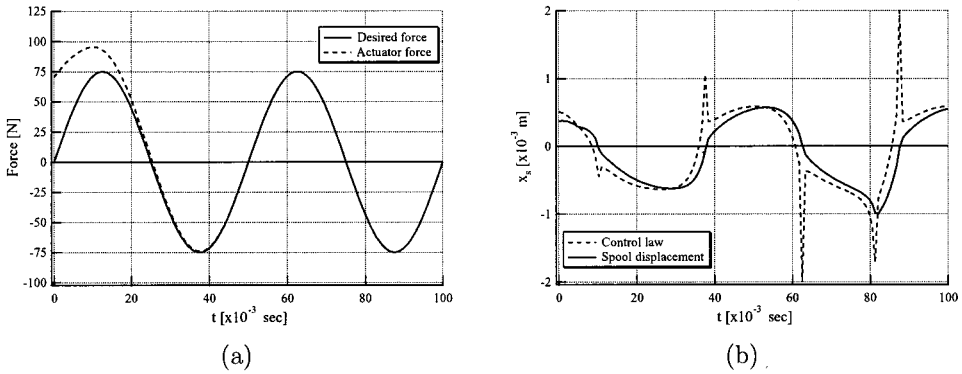

Fig. 4 Simulation results for the actuator force (a), and control law and spool displacement (b), using the full order SMC for 75 N and 20 Hz desired force, and 0.5 m tube length

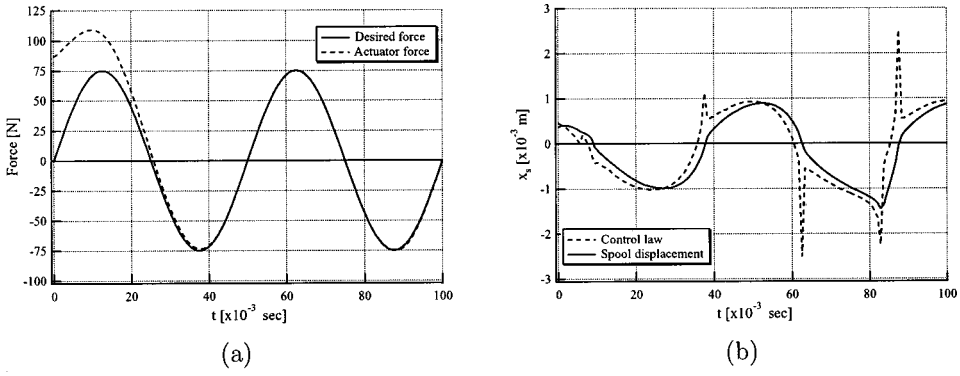

Fig. 5 Simulation results for the actuator force (a), and control law and spool displacement (b), using the full order SMC for 75 N and 20 Hz desired force, and 2 m tube length

The numerical simulation results obtained for the reduced order SMC are shown in Figs. 6 and 7. We can observe that there is a slight degradation in tracking errors when shorter tubes were used. The effect of the simplification in the controller can really be observed when longer tubes were used. We can observe that there is significant reduction in tracking performance for the 2 m tubes (see Fig. 7). In addition, the magnitude of the control current and the fluctuations in the signal become larger. Attempts to improve the tracking performance by increasing the controller gain were not fruitful because they lead to chattering.

4.2 Experimental Verification. Three sets of experiments were conducted to verify the practical utility of the proposed controllers. In the first experiment, the piston was fixed at the middle of the stroke, and the force provided by the actuator was measured using a strain gage force cell. Two configurations of the pneumatic system were tested, one with 0.5 m and the other with 2 m connecting tubes. A dither signal of 0.5 V and 300 Hz was used in the control law in order to overcome the static friction in the valve.

The measured actuator outputs for a 75 N and a 20 Hz desired

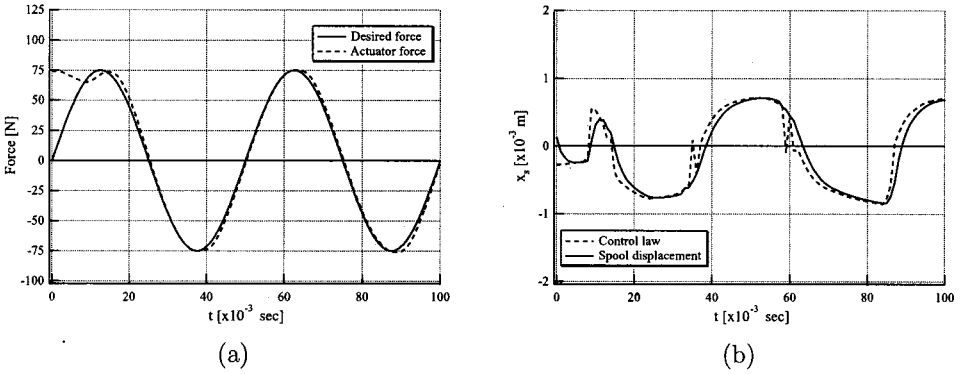

Fig. 6 Numerical results for the actuator force (a), and control law and spool displacement (b), using the reduced order SMC for 75 N and 20 Hz desired force, and 0.5 m tube length

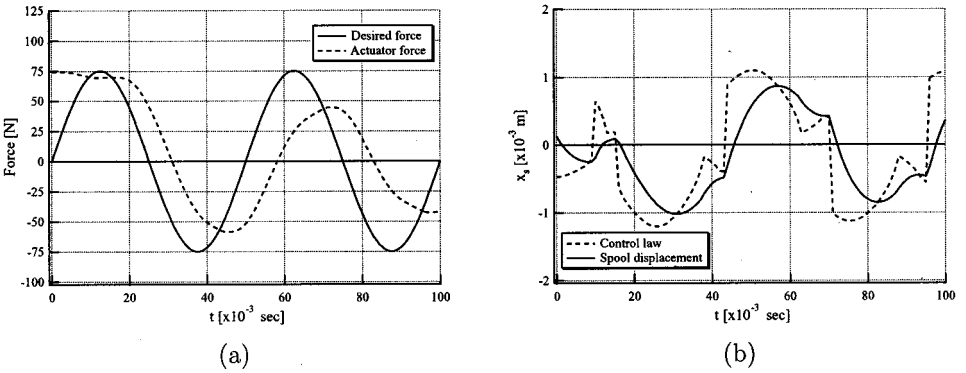

Fig. 7 Numerical results for the actuator force (a), and control law and spool displacement (b), using the reduced order SMC for 75 N and 20 Hz desired force, and 2 m tube length

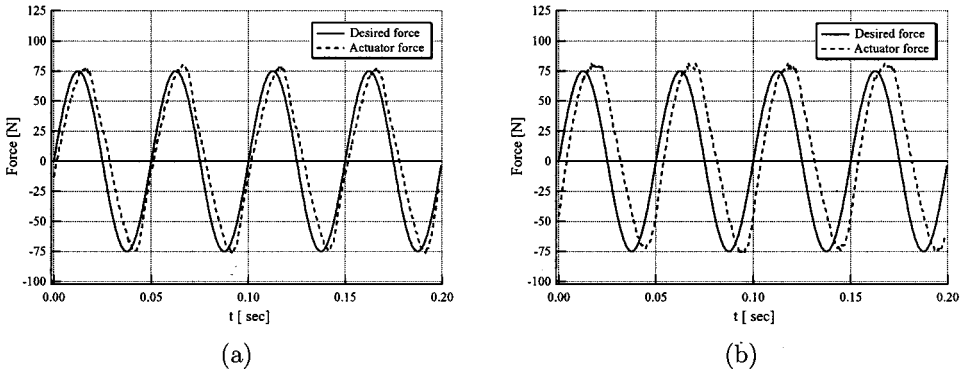

Fig. 8 Experimental values of the actuator force, using the full order SMC (a), and reduced order SMC (b), for for 75 N and 20 Hz desired force, and 0.5 m tube length

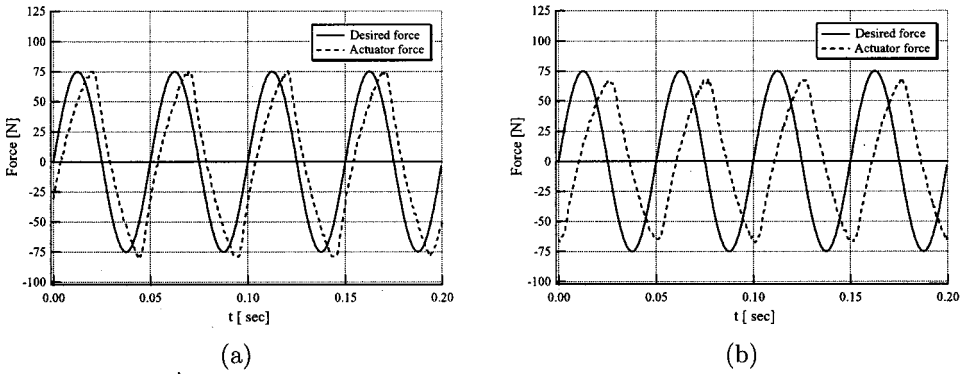

Fig. 9 Experimental values of the actuator force, using the full order SMC (a), and reduced order SMC (b), for 75 N and 20 Hz desired force, and for 2 m tube length

force and two tube lengths are presented in Figs. 8 and 9. The observed trends are similar to the ones observed during the numerical simulation. The effect of simplifying the controller is significant only when long connecting tubes are used.

Next, we present the results obtained from a set of experiments conducted to determine the frequency response of the two controllers. Throughout the experiments the piston was fixed in the middle of the stroke. The frequency response of the two controllers is presented in Figs. 10 and 11 for 0.5 m and 2 m tubes, respectively. We observed that the effect of simplifying the controller is negligible for frequencies less than 20 Hz and short tubes. However, the phase response of the reduced order controller exhibits rapid deterioration for higher frequencies even when short tubes are used (58 Hz and 53 Hz bandwidth for the full and the reduced order controllers, respectively). In addition, the full order controller is more effective at all frequencies when long tubes are used (30 Hz and 25 Hz bandwidth for the full and the reduced order controllers, respectively).

The last set of experiments was conducted to study the effect of piston motion on the performance of the controller. When the piston moves, the dynamics of the pressure in the chambers are more complex due to the changes in volume. In addition, even more complexity is introduced by the friction between the piston seals and the cylinder bore. For this purpose we designed an experimental setup that includes a mass attached to the piston and constrained by two springs (see Fig. 12). The goal of the control is to move the mass along a sinusoidal trajectory with a constant amplitude. Our purpose here is to test a force controller (not a position controller). Thus, the control action F_a is taken as the

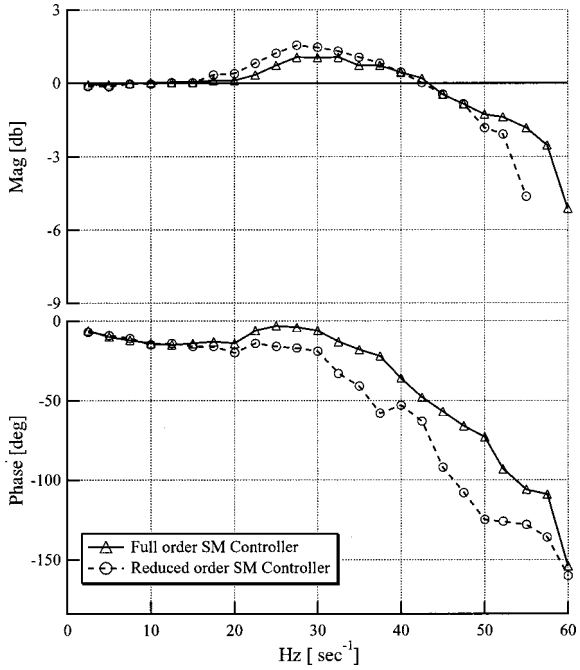

Fig. 10 Frequency response using the full and reduced order SMC, for 0.5 m tube length

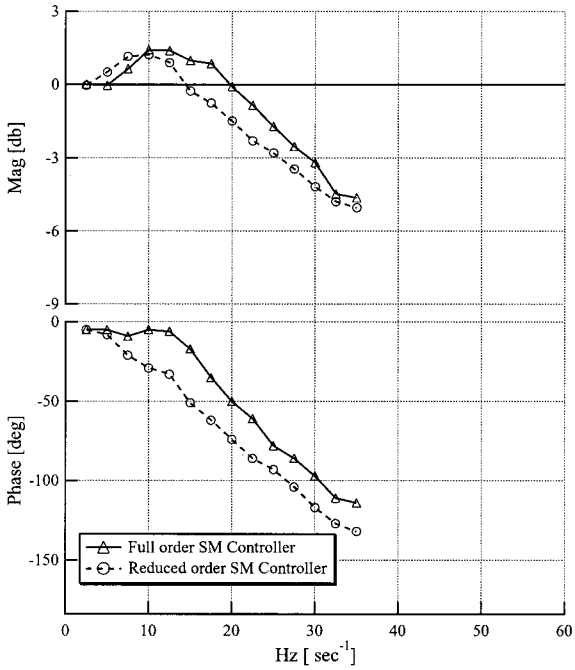

Fig. 11 Frequency response using the full and reduced order SMC, for 2 m tube length

force that is required to generate the desired displacement profile. We determine the magnitude of the required force in terms of the desired displacement, by first considering the dynamics of the load mass

$$M_L\ddot{x}+2k_{se}x=F_a \tag{28}$$

where M_L is the load mass, x is the piston displacement, and k_{se} is the spring constant. The desired sinusoidal trajectory was chosen as

$$x=a_x\sin(2\pi f_x t) \tag{29}$$

where a_x and f_x are constants. Now, the desired actuator force required to move the load can be computed as

$$F_a=2a_x(k_{se}-2\pi^2 f_x^2 M_L)\sin(2\pi f_x t). \tag{30}$$

Practically there is an upper limit to the magnitude of the force that can be applied by the pneumatic actuator. This limit, denoted by $F_{a_{\max}}$, depends on the maximum available input pressure. The upper limit on the applied force imposes an upper limit on the amplitude of the desired mass displacement ($a_{x_{\max}}$). The maximum achievable displacement amplitude for a given frequency is given by

$$a_{x_{\max}}=\left|\frac{F_{a_{\max}}}{2k_{se}-4\pi^2 f_x^2 M_L}\right|. \tag{31}$$

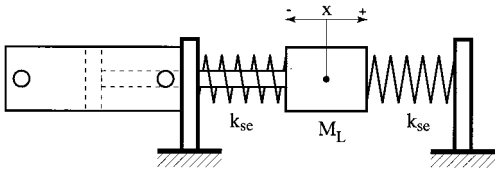

Fig. 12 Schematic representation of the moving mass experimental setup

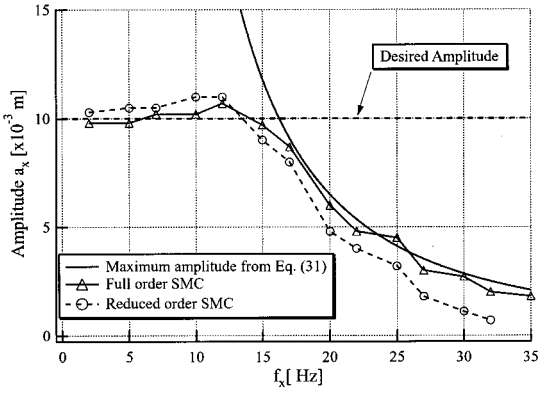

Fig. 13 Theoretical and experimental values of motion amplitude

In our experiments we used a 1 Kg mass, two identical springs with stiffness of 205 N/m, a desired a_x of 10 mm, and an input pressure of 500 kPa. Figure 13 depicts a plot of the amplitude a_x versus the input frequency f_x obtained experimentally. The experimental results demonstrate that the proposed control schemes remain to be effective when the piston moves. We can also observe that the full order controller is slightly more effective than the reduced order one. We note that the degradation in the control performance for higher frequencies is due to the limitations imposed by the maximum available input pressure, which can be observed from the figure.

5 Conclusions

A new force controller was developed for proportional-valve pneumatic actuators using the detailed mathematical model developed in the first part of this work. Due to the highly nonlinear behavior and inherent uncertainties in modeling of pneumatic systems, we chose the sliding mode control theory for controller design. The resulting controller, called the full order controller, is complex and may be expensive to use online. We also developed a reduced order controller and evaluated its advantages and disadvantages. Both controllers were tested by numerical simulation and experiments.

Our main conclusion is that detailed modeling and choosing nonlinear control provides superior performance. The bandwidth (58 Hz versus 16 Hz) of the resulting actuator is almost quadruple of the best results reported in the literature for significantly lower force levels (75 N versus 8.5 N) considered by others.

Comparison of the reduced and full order controllers revealed that the more complex control law can be justified when long connecting tubes are used, and higher actuator frequencies are desired. The advantage of using the simplified controller is to eliminate the need for intense online computations and using numerical observers for the valve spool displacement and delayed variables. Finally, we should note that even the full order controller can be implemented using currently available hardware components.

Appendix

Computation of the equivalent control from sliding mode dynamics, (Eq. (12)), requires the second derivatives of the two chamber pressures. Differentiating Eqs. (2) and (3) we obtained them as,

$$\ddot{P}_1=\frac{1}{V_1^2}\{\alpha\dot{x}^2A_1^2P_1-\dot{x}A_1[\alpha V_1\dot{P}_1+K_f(\alpha_{\text{in}}\phi_{\text{in}_1}P_s\dot{m}_r(P_s,\overline{P}_1)\overline{A}_{v1_{\text{in}}}-\alpha_{\text{ex}}\phi_{\text{ex}_1}\overline{P}_1\dot{m}_r(\overline{P}_1,P_a)\overline{A}_{v1_{\text{ex}}})]$$
$$-V_1[\alpha A_1P_1\ddot{x}+K_f(\alpha_{\text{ex}}\phi_{\text{ex}_1}\dot{\overline{P}}_1\dot{m}_r(\overline{P}_1,P_a)\overline{A}_{v1_{\text{ex}}}+\alpha_{\text{ex}}\phi_{\text{ex}_1}\overline{P}_1\dot{\overline{x}}_s\dot{m}_r(\overline{P}_1,P_a)\dot{\overline{A}}_{v1_{\text{ex}}}-P_s\alpha_{\text{in}}\phi_{\text{in}_1}\dot{\overline{x}}_s\dot{m}_r(P_s,\overline{P}_1)\dot{\overline{A}}_{v1_{\text{in}}}$$
$$-P_s\alpha_{\text{in}}\phi_{\text{in}_1}\dot{\overline{P}}_1\overline{A}_{v1_{\text{in}}}\dot{m}_r^{(0,1)}(P_s,\overline{P}_1)+\alpha_{\text{ex}}\phi_{\text{ex}_1}\overline{P}_1\dot{\overline{P}}_1\overline{A}_{v1_{\text{ex}}}\dot{m}_r^{(1,0)}(\overline{P}_1,P_a))]\} \tag{32}$$

and,

$$\ddot{P}_2=\frac{1}{V_2^2}\{\alpha\dot{x}^2A_2^2P_2+\dot{x}A_2[\alpha V_2\dot{P}_2+K_f(\alpha_{\text{in}}\phi_{\text{in}_2}P_s\dot{m}_r(P_s,\overline{P}_2)\overline{A}_{v2_{\text{in}}}-\alpha_{\text{ex}}\phi_{\text{ex}_2}\overline{P}_2\dot{m}_r(\overline{P}_2,P_a)\overline{A}_{v2_{\text{ex}}})]$$
$$+V_2[\alpha A_2P_2\ddot{x}-K_f(\alpha_{\text{ex}}\phi_{\text{ex}_2}\dot{\overline{P}}_2\dot{m}_r(\overline{P}_2,P_a)\overline{A}_{v2_{\text{ex}}}+\alpha_{\text{ex}}\phi_{\text{ex}_2}\overline{P}_2\dot{\overline{x}}_s\dot{m}_r(\overline{P}_2,P_a)\dot{\overline{A}}_{v2_{\text{ex}}}-P_s\alpha_{\text{in}}\phi_{\text{in}_2}\dot{\overline{x}}_s\dot{m}_r(P_s,\overline{P}_2)\dot{\overline{A}}_{v2_{\text{in}}}$$
$$-P_s\alpha_{\text{in}}\phi_{\text{in}_2}\dot{\overline{P}}_2\overline{A}_{v2_{\text{in}}}\dot{m}_r^{(0,1)}(P_s,\overline{P}_2)+\alpha_{\text{ex}}\phi_{\text{ex}_2}\overline{P}_2\dot{\overline{P}}_2\overline{A}_{v2_{\text{ex}}}\dot{m}_r^{(1,0)}(\overline{P}_2,P_a))]\} \tag{33}$$

where $K_f=C_fR\sqrt{T}$ is a constant, V_1 and V_2 are the chambers volume, and $\dot{m}_r^{(0,1)}$ and $\dot{m}_r^{(1,0)}$ are the partial derivatives of the reduced flow function. In Richer and Hurmuzlu [10] $\dot{m}_r(P_u,P_d)$ was defined as

$$\dot{m}_r(P_u,P_d)=\begin{cases}C_1 & \text{if } \dfrac{P_d}{P_u}\leqslant P_{cr}\\ C_2\left(\dfrac{P_d}{P_u}\right)^{1/k}\sqrt{1-\left(\dfrac{P_d}{P_u}\right)^{(k-1)/k}} & \text{if } \dfrac{P_d}{P_u}>P_{cr}.\end{cases} \tag{34}$$

Its partial derivatives are

$$\dot{m}_r^{(0,1)}(P_u,P_d)=\begin{cases}0 & \text{if } \dfrac{P_d}{P_u}\leqslant P_{cr}\\ \dfrac{C_2\left[2P_u\left(\dfrac{P_d}{P_u}\right)^{1/k}-(k+1)P_d\right]}{2kP_dP_u\sqrt{1-\left(\dfrac{P_d}{P_u}\right)^{k-1/k}}} & \text{if } \dfrac{P_d}{P_u}>P_{cr}.\end{cases} \tag{35}$$

and,

$$\dot{m}_r^{(1,0)}(P_u,P_d)=\begin{cases}0 & \text{if } \dfrac{P_d}{P_u}\leqslant P_{cr}\\ \dfrac{C_2\left[(k+1)P_d-2P_u\left(\dfrac{P_d}{P_u}\right)^{1/k}\right]}{2kP_u^2\sqrt{1-\left(\dfrac{P_d}{P_u}\right)^{k-1/k}}} & \text{if } \dfrac{P_d}{P_u}>P_{cr}.\end{cases} \tag{36}$$

The symmetry of the input and exhaust paths in the valve allows us to reduce the number of variables in control computation making the following notations

$$A_{v1_{\text{in}}}=A_{v2_{\text{ex}}}=A_{v_{\text{in}}} \tag{37}$$

$$A_{v1_{\text{ex}}}=A_{v2_{\text{in}}}=A_{v_{\text{ex}}}. \tag{38}$$

Using Eqs. (37) and (38), the derivatives of the input and exhaust air paths area become

$$\dot{A}_{v_{\text{in}}}(x_s)=-\dot{A}_{v_{\text{ex}}}(-x_s)$$
$$=\begin{cases}0 & \text{if } x_s\leqslant p_w-R_h\\ 2n_h\sqrt{R_h^2-(p_w-x_s)^2} & \text{if } x_s<p_w+R_h\\ 0 & \text{if } x_s\geqslant p_w+R_h\end{cases} \tag{39}$$

where R_h is the valve sleeve holes radius, n_h is the number of holes per air path, and $2p_w$ is the spool active width. Zero values were considered for the spool displacements corresponding to a complete obstruction of the holes cross section. For the second chamber the meaning of the input and exhaust expressions is switched, again from symmetry considerations.

Equations (32) and (33) can be written in a simpler form observing that

$$\frac{1}{V_1}[\alpha\dot{x}^2A_1^2P_1-\dot{x}A_1K_f(\alpha_{\text{in}}\phi_{\text{in}_1}P_s\dot{m}_r(P_s,\overline{P}_1)\overline{A}_{v1_{\text{in}}}$$
$$-\alpha_{\text{ex}}\phi_{\text{ex}_1}\overline{P}_1\dot{m}_r(\overline{P}_1,P_a)\overline{A}_{v1_{\text{ex}}})]=-\dot{x}A_1\dot{P}_1 \tag{40}$$

and,

$$\frac{1}{V_2}[\alpha\dot{x}^2A_2^2P_2+\dot{x}A_2K_f(\alpha_{\text{in}}\phi_{\text{in}_2}P_s\dot{m}_r(P_s,\overline{P}_2)\overline{A}_{v2_{\text{in}}}$$
$$-\alpha_{ex}\phi_{ex_2}\overline{P}_2\dot{m}_r(\overline{P}_2,P_a)\overline{A}_{v2_{ex}})]=\dot{x}A_2\dot{P}_2. \tag{41}$$

Using Eqs. (40) and (41) and grouping the terms containing the spool velocity, the pressures second derivatives become

$$\ddot{P}_1=\frac{1}{V_1}\{K_f[\alpha_{\text{in}}\phi_{\text{in}_1}P_s\dot{m}_r(P_s,\overline{P}_1)\dot{\overline{A}}_{v1_{\text{in}}}$$
$$-\alpha_{\text{ex}}\phi_{\text{ex}_1}\overline{P}_1\dot{m}_r(\overline{P}_1,P_a)\dot{\overline{A}}_{v1_{\text{ex}}}]\dot{\overline{x}}_s+K_f[\alpha_{\text{in}}\phi_{\text{in}_1}P_s\overline{A}_{v1_{\text{in}}}\dot{m}_r^{(0,1)}$$
$$\times(P_s,\overline{P}_1)-\alpha_{\text{ex}}\phi_{\text{ex}_1}\overline{P}_1\overline{A}_{v1_{\text{ex}}}\dot{m}_r^{(1,0)}(\overline{P}_1,P_a)$$
$$-\alpha_{\text{ex}}\phi_{\text{ex}_1}\dot{m}_r(\overline{P}_1,P_a)\overline{A}_{v1_{\text{ex}}}]\dot{\overline{P}}_1-(1+\alpha)A_1\dot{P}_1\dot{x}-\alpha A_1P_1\ddot{x}\} \tag{42}$$

and,

$$\ddot{P}_2=\frac{1}{V_2}\{K_f[\alpha_{\text{in}}\phi_{\text{in}_2}P_s\dot{m}_r(P_s,\overline{P}_2)\dot{\overline{A}}_{v2_{\text{in}}}$$
$$-\alpha_{\text{ex}}\phi_{\text{ex}_2}\overline{P}_2\dot{m}_r(\overline{P}_2,P_a)\dot{\overline{A}}_{v2_{\text{ex}}}]\dot{\overline{x}}_s+K_f[\alpha_{\text{in}}\phi_{\text{in}_2}P_s\overline{A}_{v2_{\text{in}}}\dot{m}_r^{(0,1)}$$
$$\times(P_s,\overline{P}_2)-\alpha_{\text{ex}}\phi_{\text{ex}_2}\overline{P}_2\overline{A}_{v2_{\text{ex}}}\dot{m}_r^{(1,0)}(\overline{P}_2,P_a)$$
$$-\alpha_{\text{ex}}\phi_{\text{ex}_2}\dot{m}_r(\overline{P}_2,P_a)\overline{A}_{v2_{\text{ex}}}]\dot{\overline{P}}_2+(1+\alpha)A_2\dot{P}_2\dot{x}+\alpha A_2P_2\ddot{x}\}. \tag{43}$$

Substituting Eqs. (42) and (43) in Eq. (12), and using the derivative of the spool displacement, $\dot{x}_s$, from Eq. (8) we obtained an equation that can be solved for the valve input u. The control law obtained in this way represents the equivalent control u_{eq} from Eq. (13)

$$u_{eq}=\frac{\frac{1}{\tau_v}(A_1b_{11}-A_2b_{21})\overline{x_s}-A_1b_{12}\overline{\dot{P}_1}+A_2b_{22}\overline{\dot{P}_2}+A_1b_{13}+A_2b_{23}-c_1}{\frac{1}{\tau_v}(A_1b_{11}-A_2b_{21})} \tag{44}$$

where we used Eqs. (37) and (38), and the following notations were made

$$b_{11}=\frac{K_f}{V_1}[\alpha_{\text{in}}\phi_{\text{in}_1}P_s\dot{m}_r(P_s\overline{P_1})\overline{\dot{A}_{v_{\text{in}}}}-\alpha_{\text{ex}}\phi_{\text{ex}_1}\overline{P_1}\dot{m}_r(\overline{P_1},P_a)\overline{\dot{A}_{v_{\text{ex}}}}] \tag{45}$$

$$b_{12}=\frac{K_f}{V_1}[\alpha_{\text{in}}\phi_{\text{in}_1}P_s\overline{A_{v_{\text{in}}}}\dot{m}_r^{(0,1)}(P_s,\overline{P_1})-\alpha_{\text{ex}}\phi_{\text{ex}_1}\overline{P_1}\overline{A}_{v1_{\text{ex}}}\dot{m}_r^{(1,0)}\times(\overline{P_1},P_a)-\alpha_{\text{ex}}\phi_{\text{ex}_1}\dot{m}_r(\overline{P_1},P_a)\overline{A_{v_{\text{ex}}}}] \tag{46}$$

$$b_{13}=(1+\alpha)A_1\dot{P}_1\dot{x}+\alpha A_1P_1\ddot{x} \tag{47}$$

$$b_{21}=\frac{K_f}{V_2}[\alpha_{\text{in}}\phi_{\text{in}_2}P_s\dot{m}_r(P_s,\overline{P_2})\overline{\dot{A}_{v_{\text{ex}}}}-\alpha_{\text{ex}}\phi_{\text{ex}_2}\overline{P_2}\dot{m}_r(\overline{P_2},P_a)\overline{\dot{A}_{v_{\text{in}}}}] \tag{48}$$

$$b_{22}=\frac{K_f}{V_2}[\alpha_{\text{in}}\phi_{\text{in}_2}P_s\overline{A_{v_{\text{ex}}}}\dot{m}_r^{(0,1)}(P_s,\overline{P_2})-\alpha_{\text{ex}}\phi_{\text{ex}_2}\overline{P_2}\overline{A}_{v_{\text{in}}}\dot{m}_r^{(1,0)}\times(\overline{P_2},P_a)-\alpha_{\text{ex}}\phi_{\text{ex}_2}\dot{m}_r(\overline{P_2},P_a)\overline{A_{v_{\text{in}}}}] \tag{49}$$

$$b_{23}=(1+\alpha)A_2\dot{P}_2\dot{x}+\alpha A_2P_2\ddot{x} \tag{50}$$

and,

$$c_1=\lambda(A_1\dot{P}_1-A_2\dot{P}_2-\dot{F}_d-\beta\ddot{x})-\beta x^{(3)}-\ddot{F}_d. \tag{51}$$

The equivalent control expression, Eq. (44), contains the valve spool position x_s delayed with the time τ, required by the pressure wave to travel the connecting tubes. Usually its value cannot be directly measured, thus it cannot be used as a feedback variable. Consequently, it should be estimated by numerical integration or by using a nonlinear observer. The estimated value can then be used in the computation of $\overline{A_{v_{\text{in}}}}$ and $\overline{A_{v_{\text{ex}}}}$ also. The pressure derivatives appears as both nondelayed and delayed values. The nondelayed values can be computed using Eqs. (2) and (3), respectively, and a numerical delay filter can then be applied for the delayed values. The transfer function for such a filter is $T_d(s)=e^{-\tau s}$, which can be approximated as

$$T_d(s)=\frac{1}{\frac{1}{2}\tau^2s^2+\tau s+1}. \tag{52}$$

The state equations for this filter can be expressed as

$$\dot{x}_1=x_2 \tag{53}$$

$$\dot{x}_2=-\frac{2}{\tau^2}x_1-\frac{2}{\tau}x_2+\frac{2}{\tau^2}v \tag{54}$$

and

$$y=x_1 \tag{55}$$

were v is the input, x_1 and x_2 are the filter's state variables, and y is the output.

The computation of the term c_1 requires the first and second derivatives of the desired force F_d, and also the second and third derivatives of the piston position x. The velocity and acceleration of the piston are also required for b_{13} and b_{23} terms. While the force derivatives are input variables, and they are given in the vector $\mathbf{F_d}$, the position derivatives are state variables, and they have to be measured or estimated using numerical methods. Numerical differentiation is particularly sensitive to noisy input data, thus requiring additional noise filters. A digital differentiating filter combined with a second order low-pass filter was design and tested numerically and in experiments. Its transfer function is

$$T(s)=\frac{\omega^2s}{s^2+2\zeta\omega s+\omega^2} \tag{56}$$

where ω is the filter corner frequency, and ζ is the damping coefficient. The state equations for the filter were obtained using simulation diagram method as

$$\dot{x}_1=x_2 \tag{57}$$

$$\dot{x}_2=-2\zeta\omega x_2-\omega^2x_1+v \tag{58}$$

and

$$y=\omega^2x_2 \tag{59}$$

were v is the input, x_1 and x_2 are the filter's state variables, and y is the output. Using the position x as the input variable and a sequence of two such filters, we obtained both the velocity and the acceleration of the piston, with low noise and very small phase lag. Both the measurement and the numerical estimation of $x^{(3)}$ present difficulties related to the required instrumentation or the noise and phase shift in the numerical computation. Consequently, we decided to eliminate the corresponding term from Eq. (51).

References

[1] Mannetje, J. J., 1981, ''Pneumatic Servo Design Method Improves System Bandwidth Twenty-fold,'' Control. Eng., pp. 79–83.

[2] Bobrow, J. E., and Jabbari, F., 1991, ''Adaptive Pneumatic Force Actuation and Position Control,'' ASME J. Dyn. Syst., Meas., Control, **113**, pp. 267–272.

[3] Ferraresi, C., Giruado, P., and Quaglia, G., 1994, ''Non-Conventional Adaptive Control Of Servopneumatic Unit For Vertical Load Positioning,'' *Proceedings of the 45th National Conference on Fluid Power*.

[4] McDonell, B. W., and Bobrow, J. E., 1993, ''Adaptive Traking Control of an Air Powered Robot Actuator,'' ASME J. Dyn. Syst., Meas., Control, **115**, pp. 427–433.

[5] Ben-Dov, D., and Salcudean, S. E., 1995, ''A Force-Controlled Pneumatic Actuator,'' IEEE Trans. Rob. Autom., **11**, No. 6, pp. 906–911.

[6] Richard, E., and Scavarda, S., 1996, ''Comparison Between Linear and Nonlinear Control of an Electropneumatic Servodrive,'' ASME J. Dyn. Syst., Meas., Control, **118**, pp. 245–118.

[7] Arun, P. K., Mishra, J. K., and Radke, M. G., 1994, ''Reduced Order Sliding Mode Control for Pneumatic Actuator,'' IEEE Trans. Control Syst. Technol., **2**, No. 3, pp. 271–276.

[8] Tang, J., and Walker, G., 1995, ''Variable Structure Control of a Pneumatic Actuator,'' Trans. ASME, **117**, pp. 88–92.

[9] Pandian, S. R., Hayakawa, Y., Kanazawa, Y., Kamoyama, Y., and Kawamura, S., 1997, ''Practical Design of a Sliding Moth Controller for Pneumatic Actuators,'' ASME J. Dyn. Syst., Meas., Control, **119**, 666.

[10] Richer, E., and Hurmuzlu, Y., 1999, ''A High Performance Pneumatic Force Actuator System: Part I—Nonlinear Mathematical Model,'' ASME J. Dyn. Syst., Meas. Control, **122**, pp. 416–425.

[11] Slotine, J. E., and Li, Y., 1991, *Applied Nonlinear Control*, Prentice-Hall, New Jersey.